Precise Access to the Molecular-Frame Complex Recombination Dipole through High-Harmonic Spectroscopy

S. B. Schoun, A. Camper, P. Salières, R. R. Lucchese, P. Agostini, and L. F. DiMauro

Phys. Rev. Lett. **118**, 033201 — Published 19 January 2017

DOI: 10.1103/PhysRevLett.118.033201

Precise access to the molecular-frame complex recombination dipole through high-harmonic spectroscopy

S. B. Schoun,[1] A. Camper,[1,*] P. Salières,[2] R. R. Lucchese,[3] P. Agostini,[1] and L. F. DiMauro[1]

[1] *Department of Physics, The Ohio State University, Columbus, Ohio 43210, USA*
[2] *LIDYL, CEA, CNRS, Université Paris-Saclay, CEA Saclay, 91191 Gif-Sur-Yvette, France*
[3] *Department of Chemistry, Texas A&M University, College Station, Texas 77843, USA*

(Dated: December 20, 2016)

We report on spectral intensity and group delay measurements of the highest-occupied molecular-orbital (HOMO) recombination dipole moment of N_2 in the molecular-frame using high harmonic spectroscopy. We take advantage of the long-wavelength 1.3 μm driving laser to isolate the HOMO in the near threshold region, 19–67 eV. The precision of our group delay measurements reveals previously-unseen angle-resolved spectral features associated with autoionizing resonances, and allows quantitative comparison with cutting-edge correlated 8-channel photoionization dipole moment calculations.

PACS numbers: 32.70.-n, 42.65.Ky, 42.65.Re

Molecular-frame photoionization and recombination [1–4] contains a rich abundance of information about orbital structure and dynamics that is washed-out in traditional [5] extreme-ultraviolet (XUV) spectroscopy of randomly-oriented molecules. Knowledge of molecular orientation in most valence-shell photoionization experiments requires using laser-induced impulsive pre-alignment techniques [6] when the ion does not dissociate, thus necessitating short-pulsed XUV sources for spectroscopy like high-order harmonic generation (HHG) [7], femtosecond sliced synchrotrons [8], or free-electron lasers [9]. Among these, HHG is unique in that it allows for complete characterization of the complex transition dipole matrix element in both magnitude (the cross section) and *phase*. In scattering terms, photoionization and recombination are described as half-collisions, whereby a continuum electron wavepacket acquires an extra phase while it is temporarily trapped or repulsed by the ionic potential [10]. This simple picture must be amended if the dipole phase is not linear with frequency, as occurs across resonance features like multi-center interferences [11], Cooper minima [12], shape resonances, and autoionization resonances [13], in which case the electron wavepacket is both delayed and reshaped [12, 14]. In the molecular frame, such spectral features may have strong angular variations due to the effective inter-nuclear distance and shape of the potential seen by the electron at a given angle. In this letter, we show that the dipole phase is also a sensitive probe of electron correlation by performing an accurate experimental characterization of both the magnitude and group delay of nitrogen's dipole moment. Using mid-infrared (1.3 μm wavelength) driven HHG spanning the vicinity of the $3\sigma_g$ shape resonance (pathological region where resonances strongly distort the dipole), our results provide a benchmark for advanced theoretical predictions.

Instead of using the XUV to photoionize nitrogen, here the XUV is *generated* in aligned N_2, allowing us to study its dipole through the recombination process in which an electron wavepacket (EWP) is prepared in the continuum by strong-field ionization and accelerated back to the ion by the intense laser field [15, 16], a technique that has come to be known as high harmonic spectroscopy (HHS). When the harmonic process is driven in the tunneling ionization regime (the Keldysh parameter [17] is $\gamma = 0.62$ for our experimental conditions) without ground-state depletion, the associated recombination dipole is equivalent to the time-reversed photoionization dipole [18–20]. HHS has been previously applied to N_2 [21, 22] in the context of molecular tomography [21, 23], although driven with Ti:Sapphire lasers (0.8 μm wavelength). In such conditions, HHS is plagued by the intricate contributions of the two highest-occupied molecular orbitals (noted HOMO and HOMO–1 respectively) [24], preventing access to precise molecular dipoles over an extended spectral range. The use here of a long-wavelength mid-IR driving pulse has several key advantages. Due to the favorable λ^2-wavelength scaling of the harmonic cutoff energy [15, 16], our spectrum covers a broad bandwidth extending beyond 90 eV, almost twice the cutoff reached at 0.8 μm, putting the shape resonance well-within the harmonic plateau region, while simultaneously allowing us to maintain a low laser intensity (1.3×10^{14} W/cm^2), drastically reducing the contribution of inner-shell orbitals and singling-out the HOMO [24]. Moreover, the smaller harmonic spacing provides a 60% increase in sampling resolution compared to the earlier studies. As a result, our experimental approach improves the measurement precision of molecular dipole moments and reveals previously unseen structures associated with autoionization resonances, illustrating the ability of HHS to test the accuracy of molecular-frame photoionization calculations.

The main experimental apparatus has been described in refs. [12, 25]. Briefly, a 1 kHz repetition rate

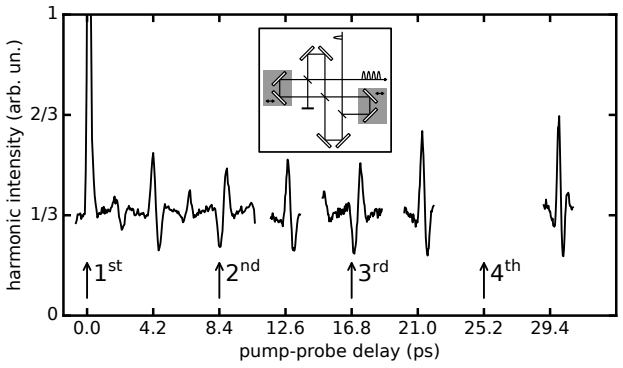

FIG. 1. HHG spectral intensity at 32 eV from N_2 as a function of the pump-probe delay. The inset shows the nested interferometer which creates the 4-kicker pulse train used to populate a coherent rotational wavepacket in the molecular ensemble. Each arrow indicates the delay of one kick. At 0 delay, the huge enhancement is due to the pump-probe temporal overlap. At 8.4 ps delay (respectively 16.8 ps), the trace was recorded in the absence of the second (resp. third) kick.

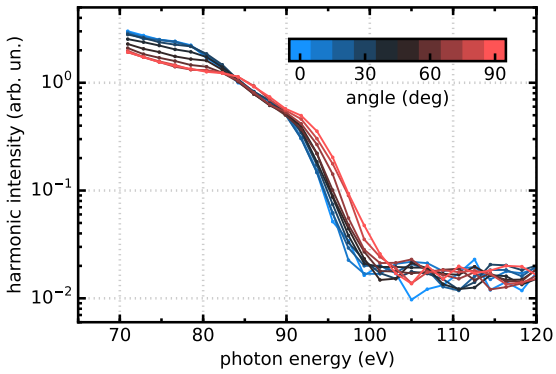

FIG. 2. (Color online) N_2 harmonic spectral intensity in the cutoff region. Alignment angles are shown from 0° (light blue) to 90° (light red). Each harmonic order is integrated for clarity.

Ti:Sapphire laser with 6 mJ pulse energy is used to pump an optical parametric amplifier (OPA). The 1.3 μm signal output of the OPA, with 1.2 mJ pulses of 65 fs duration, is split into two arms of a Mach-Zehnder interferometer: one arm drives HHG in a continuous gas jet backed with 4 bar of N_2 supplied through a 150 μm diameter nozzle, and the other arm is used to characterize the HHG group delay using the reconstruction of attosecond beating by interference of two-photon transitions (RABBITT) [26, 27] method. In the far field, a thin metallic foil absorbs the driving field, and an iris acts as a spatial filter of the HHG emission. The harmonics are then detected with a time-of-flight magnetic-bottle electron spectrometer (MBES) [28].

In order to achieve a high degree of molecular alignment ($\langle\cos^2(\theta)\rangle = 0.52$ estimated from linear-rotor impulsive alignment simulations) while maintaining the high gas density needed for efficient phase matching, we incorporate the repetitive-kicking technique [29] using a nested four-pulse kicker interferometer, see Fig. 1. The 0.8 μm depleted pump output of the OPA is split into four delayed pulses by the nested interferometer and focused into the generation gas to prepare the molecular alignment. The delay between each consecutive pulse in the train of kicks is set to one full revival period of N_2 (8.4 ps). The delay between the last kick and the generation probe pulse is set to the peak of the next half-revival. A half-wave plate in the alignment beam controls the angle between the probe polarization and the axis of symmetry of the molecular ensemble, referred to as the alignment angle.

To perform clean HHS, we need to ensure that the measured dipole comes from a single orbital. Indeed, significant contributions from the HOMO–1 have been evident mainly in the cutoff region [21–23, 30]. To this end, we compare the harmonic spectral intensity measured for ten alignment angles between 0° and 90° in 10° increments in the upper plateau and cutoff region, as measured through a 150 nm thick zirconium filter that passes the harmonics above ~60 eV (see Fig. 2). Each cutoff spectrum is corrected for the apparatus response function by dividing by the Zr transmittance and the cross section of the MBES argon detection gas. At low energies, the HHG yield is strongest at 0° and decreases with increasing alignment angle, exactly as expected for the HOMO, which has a σ orbital symmetry, giving it the highest probability along the molecular axis for both recombination and strong-field ionization. However, for energies near and above the cutoff at 90 eV, there is a reversal in the HHG yield as a function of alignment angle, with the highest yield occurring for 90°. This cutoff extension is consistent with the onset of significant contributions from the HOMO–1, which has a π orbital symmetry, giving it the highest probability perpendicular to the molecular axis for both recombination and strong-field ionization, and whose ionization potential energy ($I_p = 17.2$ eV) is higher than that of the HOMO ($I_p = 15.58$ eV), giving it a slightly higher effective cutoff [22, 24]. This extension and reversal in the cutoff, attributed to the HOMO–1, has previously been observed in N_2 at 0.8 μm, albeit at a much lower energy [30, 31]. In our case, the lack of any such reversal below 80 eV, see Fig. 2 and Fig. 3(a), we take to be a strong indication that the HOMO–1 does not contribute significantly below the cutoff.

We now turn to the advanced characterization in magnitude and phase of the HOMO dipole in the 20–70 eV region, as measured through a 200 nm thick aluminum filter. In Fig. 3(a), we show the N_2 plateau harmonic spectral intensity as measured with the Al filter. The intensity of each harmonic order is normalized by the value measured at the same energy when generating in unaligned N_2 to completely calibrate out the detector

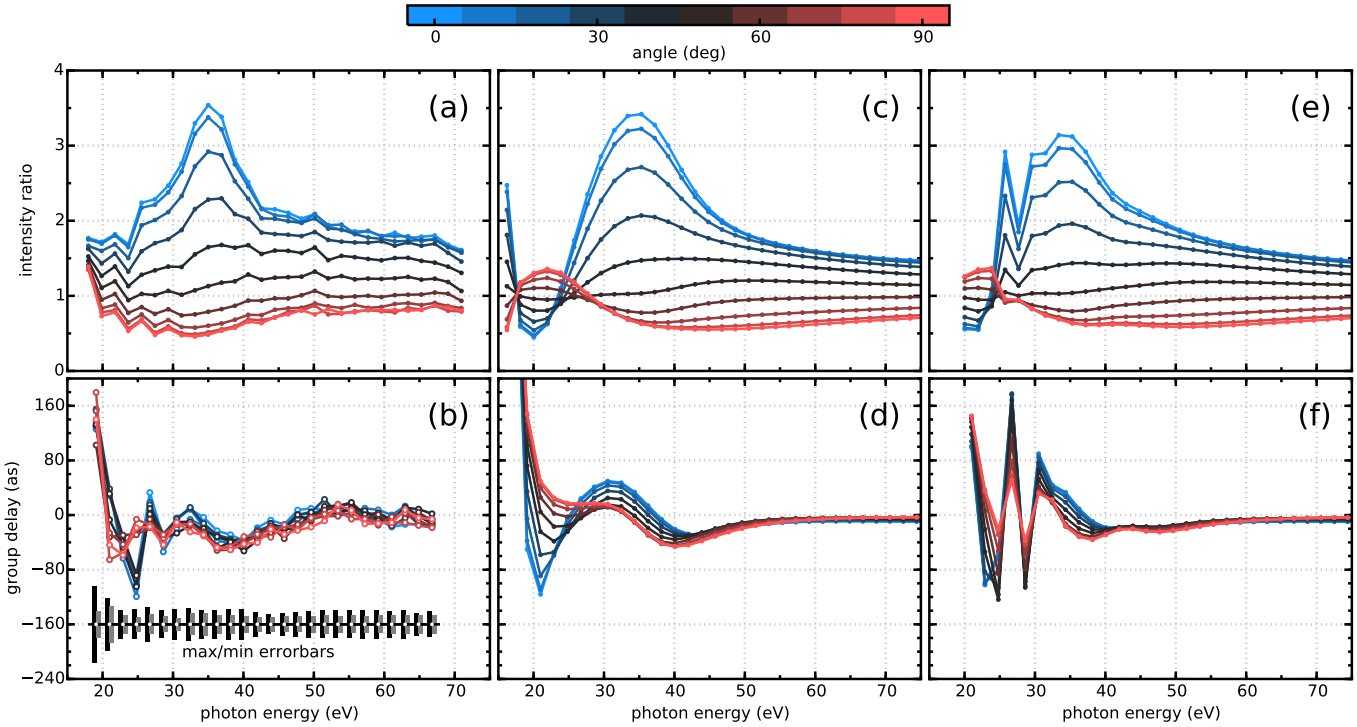

FIG. 3. (Color online) Complex dipole of N_2. Harmonic spectral intensity normalized to the isotropic yield for different alignment angles from 0° (light blue) to 90° (light red) as measured experimentally (a) and as predicted by theory using 3 (c) and 8 (e) channel angle-convolved photoionization dipole moments. Dipole group delay as measured experimentally (b) and as predicted by theory using 3 (d) and 8 (f) channels. In (b) only the largest and smallest errorbars are shown and offset for clarity. The standard error of the experimental group delay is estimated from the fit to the RABBITT sideband oscillations.

response, including removing unwanted cyclotron modulation effects in the MBES at low energies. This normalization also removes the energy-dependence of the EWP.

In the RABBITT experiment, the quantity that is directly measured is not the spectral phase, $\varphi(\omega)$, itself, but rather a discrete-difference approximation to the group delay (GD), $\mathrm{d}\varphi(\omega)/\mathrm{d}\omega$, which is shown in Fig. 3(b). The dipole GD is extracted from the total GD of the harmonics by subtracting GD contributions of the EWP calculated classically, the Al filter, and the atomic delay of the detection gas, akin to the procedure described in ref. [12]. The experimental results are obtained by stitching together two sets of group delay measurements. Between 18 and 40 eV, the detection gas is argon. Above 40 eV, the cross section in argon becomes small due to a Cooper minimum [12], thus neon is used as the detection gas above 32 eV. For the 5 sidebands in the overlap region (32 to 40 eV), the agreement between the two datasets is excellent and we present the average value over the two measurements. Also, since our setup only allows for the determination of the GD up to an unknown absolute constant, the constant offset of each curve is set to minimize the quadratic difference to the 3-channel model predictions, discussed below, in the 32–67 eV spectral region, where the experimental results and the predictions of both models are relatively flat.

We now compare in Fig. 3 the measured angularly-resolved dipole intensities and group delays, below the harmonic cutoff, with the predictions of a theoretical model utilizing two photoionization dipoles of increasing complexity. A detailed description of how these two dipoles have been calculated is presented in the Supplementary Information [32]. We start with accurate calculations of the parallel component (meaning the electron propagates parallel to the polarization vector of the XUV field) of the molecular-frame scattering-wave dipole matrix element [44, 45], $d_{\parallel}(\theta)$, describing the removal of an electron from the $3\sigma_g$ orbital of N_2 leading to the $X\,^2\Sigma_g^+$ state of N_2^+. The dipoles are calculated with fixed nuclei at a separation distance of $R = 1.09768$ Å, and incorporate electron correlations among 3 or 8 total channels (states). The channels are included following a decreasing order in the associated coupling strength. Therefore, the 3-channel dipole includes autoionization resonances from threshold up to 19 eV, and the 8-channel dipole includes autoionization resonances up to 34 eV. Note that, up to now in HHS, the very qualitative comparison was restricted to single or 3 channel calculations. We assume that, at the scale of the optical cycle, the nuclear vibrational wavepacket populated in the $X\,^2\Sigma_g^+$ state of the ion does not evolve significantly and therefore the nuclear auto-correlation function is set to 1 [22]. In or-

der to account for imperfect alignment in the theoretical model, we calculate the convolution of the molecular-frame dipole with the alignment distribution $\rho(\theta)$:

$$\widetilde{d}_{\parallel}(\alpha) = \int_0^{\pi} \mathrm{d}\theta' \int_0^{2\pi} \mathrm{d}\phi' \sqrt{\Gamma(\theta')}\, d_{\parallel}(\theta')\, \rho\big[\theta(\theta',\phi',\alpha)\big] \sin(\theta'), \quad (1)$$

where α is the angle between the pump and probe polarizations, θ' and ϕ' are the spherical angular coordinates of the molecular axis in the probe frame, and θ is the polar coordinate of the molecular axis in the pump frame given by $\cos(\theta) = \cos(\alpha)\cos(\theta') + \sin(\alpha)\sin(\theta')\cos(\phi')$ [19]. In the theoretical model, the molecular dipole is weighted by the strong-field ionization amplitude $\sqrt{\Gamma(\theta)}$ that is angle dependent and cannot be factorized out. In the calculation of Eq. (1) we use the experimental rate of ref. [46] described as follows: $\Gamma(\theta) = \frac{1+\epsilon\cos^2(\theta)}{1+\epsilon}$, with $\epsilon = 2.3$. The alignment angular distribution $\rho(\theta)$, shown in Supplementary Information [32] Fig. S1, is calculated from a linear-rotor molecular-alignment simulation using the time-dependent Schrödinger equation [47] for our multi-kick experimental conditions, estimated to consist of: a gas rotational temperature of 150 K, kicking-pulse intensities of 2×10^{13} W/cm^2, and pulse durations of 65 fs. Figure 3(c–f) shows the results of the model calculations, Eq. (1), for the angle-convolved 3-channel and 8-channel dipole.

The overall agreement of the spectral intensity and group delay between the experiment and the 3-channel model in Fig. 3 is good, and the experimental agreement with the 8-channel model is even better, for all alignment angles. See also Fig. 4 for a direct overlay of the models and experiment for the 0° case. The 3-channel dipole calculations are in particularly good agreement with the experiment above 30 eV. Notice that at 0° the spectrum is peaked around 35 eV, revealing the wide shape resonance in the HOMO dipole [24, 44, 48, 49], although it is shifted relative to the unconvolved theoretical dipole, which peaks at 31 eV. In this spectral range, our results are also in qualitative agreement with experimental photoionization cross sections from aligned N_2 [4]. Below 30 eV, the strong oscillations in the group delay measurement associated with deviations in the bell-shape intensity curve are not found in the 3-channel predictions. The 8-channel calculations predict these features, related to autoionization resonances, much better. These narrow autoionization resonances, observed for the first time in HHS from N_2, are not completely resolved at this harmonic spacing, but are still clearly evident and contribute to the zig-zag behavior in both the spectrum and group delay between 20 and 30 eV. The zig-zag feature might also be contaminated by the Fano resonance in the argon detection gas around 26 eV [50], however, the strong angular dependence of our group delay measurements shows that the detection gas is not the main source of this zig-zag shape. Based on the comparison with theory, the largest feature in the experimental group delay at

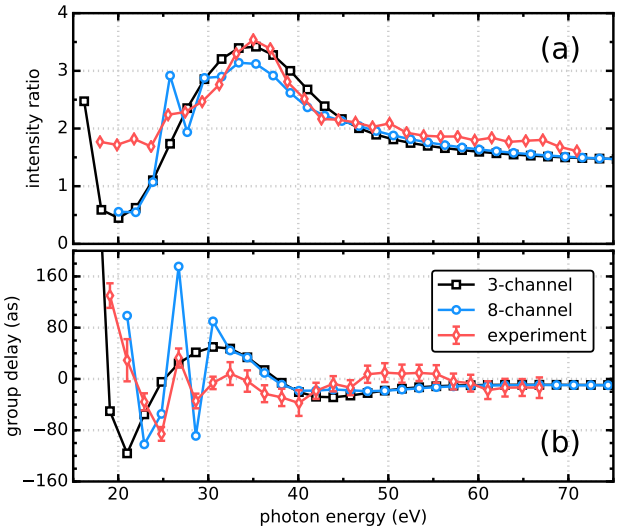

FIG. 4. (Color online) Complex dipole of N_2 along the internuclear axis. Direct comparison between experiment and 3- and 8-channel model of the dipole normalized intensity (a) and group delay (b) for the ensemble of N_2 aligned at 0°.

24.8 eV, which shows up as a dip in the GD for small angles, is caused by the shape resonance, heavily distorted by the autoionization resonances and shifted by the angular convolution. There is, however, strong disagreement in the spectral intensity for energies lower than 27 eV, where the models predict a reversal in the dependence on alignment angle that is not seen in the experiment. A few prior experimental studies using 0.8 μm [21, 22, 30, 49, 51] have investigated the spectral intensity behavior in this low energy region, and all of them show results consistent with our experiment, although we note that the model is rather sensitive in this energy region to the exact shape of the alignment distribution that is used in the angular convolution, see Eq. (1). Other possible sources of discrepancy between experiment and theory could be the perpendicular polarization component of the XUV for alignment angles other than exactly 0° or 90° [52], or nuclear vibrations [53], both of which are neglected in the present model.

Interestingly, there is a striking difference between our group delay measurement and previous findings at 0.8 μm [21, 22]. In the latter, the group delay at 90° is smaller than at 0°. In our measurements at 1.3 μm, the group delay at different alignment angles are mainly identical above 30 eV but at 24 eV the group delay at 0° is much smaller than at 90°. Since previous results at 0.8 μm were interpreted as footprints of the HOMO–1 in this spectral range, this difference can be considered as another proof of only the HOMO contributing to the *plateau* region when longer-wavelength mid-IR lasers drive the HHG process.

The precise dipole intensity and group delay measurements combined with advanced theoretical calculations

presented here pave the way towards time-resolved studies of electron correlations through HHS. Sharpening our knowledge of photoionization dipoles in regions where complicated multi-electron interactions are found, up to the point where the contributions of each channel are well characterized, is a prerequisite for further time-resolved ultrafast control and investigation. For example, although shape resonances are actually single-electron phenomena, their existence in one ionization channel can amplify electron correlations at the resonance energy because the continuum electron, which is briefly trapped locally near the ion, has more time to interact with the other electrons before it escapes to large distances [54–56]. Determining what degree of correlation and how many (and which) states should be included to properly describe valence-shell photoionization still remains a challenge for theory, emphasizing the need for more sensitive and alternate experimental measurements of these highly-structured resonances. Our results suggest that HHS fills this void.

In conclusion, we report on precise spectral intensity and group delay investigations of HHS at 1.3 μm from aligned N_2 with a cutoff as high as 90 eV. This driving wavelength allows us to measure a single-orbital dipole with fine sampling over an unprecedented 50 eV spectral bandwidth. We find good agreement between our experimental results and the most advanced photoionization dipole calculations to-date in a pathological region combining a shape resonance and autoionizing resonances. The latter features, observed for the first time in N_2 HHS, required elaborated photoionization dipole calculations with 9 active electrons and autoionization states, bringing the capabilities of HHS to a new stage. These results open new perspectives for future attosecond time-resolved high harmonic spectroscopy studies where more complicated correlated electron and light nuclei dynamics occur between ionization and recombination of the EWP.

We would like to thank Robert R. Jones for providing us with his linear-rotor molecular-alignment code. This work is supported by the US Department of Energy, Office of Science, Office of Basic Energy Sciences under contracts DE-FG02-04ER15614 and DE-FG02-06ER15833. A.C. acknowledges support from the collaboration program CNRS-PICS 2010–2012 under no. 5460. The authors acknowledge the technical assistance of Dietrich Kiesewetter and Tim Gorman.

* camper.22@osu.edu

[1] D. Dill, J. Chem. Phys. **65**, 1130 (1976).
[2] D. Dill, J. Siegel, and J. L. Dehmer, J. Chem. Phys. **65**, 3158 (1976).
[3] C. Jin, A.-T. Le, S.-F. Zhao, R. R. Lucchese, and C. D. Lin, Phys. Rev. A **81**, 033421 (2010).
[4] A. Rouzée, F. Kelkensberg, W. K. Siu, G. Gademann, R. R. Lucchese, and M. J. J. Vrakking, J. Phys. B **45**, 074016 (2012).
[5] M. Ilchen, S. Deinert, L. Glaser, F. Scholz, J. Seltmann, P. Walter, and J. Viefhaus, J. Phys. B **45**, 225102 (2012).
[6] H. Stapelfeldt and T. Seideman, Rev. Mod. Phys. **75**, 543 (2003).
[7] I. Thomann, R. Lock, V. Sharma, E. Gagnon, S. T. Pratt, H. C. Kapteyn, M. M. Murnane, and W. Li, J. Phys. Chem. A **112**, 9382 (2008).
[8] R. W. Schoenlein, S. Chattopadhyay, H. H. W. Chong, T. E. Glover, P. A. Heimann, C. V. Shank, A. A. Zholents, and M. S. Zolotorev, Science **287**, 2237 (2000).
[9] A. Rouzée, P. Johnsson, L. Rading, A. Hundertmark, W. Siu, Y. Huismans, S. Düsterer, H. Redlin, F. Tavella, N. Stojanovic, A. Al-Shemmary, F. Lépine, D. M. P. Holland, T. Schlatholter, R. Hoekstra, H. Fukuzawa, K. Ueda, and M. J. J. Vrakking, J. Phys. B **46**, 164029 (2013).
[10] J. M. Dahlström, A. L'Huillier, and A. Maquet, J. Phys. B **45**, 183001 (2012).
[11] H. D. Cohen and U. Fano, Phys. Rev. **150**, 30 (1966).
[12] S. B. Schoun, R. Chirla, J. Wheeler, C. Roedig, P. Agostini, L. F. DiMauro, K. J. Schafer, and M. B. Gaarde, Phys. Rev. Lett. **112**, 153001 (2014).
[13] S. Haessler, B. Fabre, J. Higuet, J. Caillat, T. Ruchon, P. Breger, B. Carré, E. Constant, A. Maquet, E. Mével, P. Salières, R. Taïeb, and Y. Mairesse, Phys. Rev. A **80**, 011404 (2009).
[14] S. Haessler, V. Strelkov, L. B. E. Bom, M. Khokhlova, O. Gobert, J.-F. Hergott, F. Lepetit, M. Perdrix, T. Ozaki, and P. Salières, New J. Phys. **15**, 013051 (2013).
[15] K. J. Schafer, B. Yang, L. F. DiMauro, and K. C. Kulander, Phys. Rev. Lett. **70**, 1599 (1993).
[16] P. B. Corkum, Phys. Rev. Lett. **71**, 1994 (1993).
[17] L. V. Keldysh, Sov. Phys. JETP **20**, 1307 (1965).
[18] A.-T. Le, R. D. Picca, P. D. Fainstein, D. A. Telnov, M. Lein, and C. D. Lin, J. Phys. B **41**, 081002 (2008).
[19] A.-T. Le, R. R. Lucchese, S. Tonzani, T. Morishita, and C. D. Lin, Phys. Rev. A **80**, 013401 (2009).
[20] M. V. Frolov, N. L. Manakov, T. S. Sarantseva, and A. F. Starace, Phys. Rev. A **83**, 043416 (2011).
[21] S. Haessler, J. Caillat, W. Boutu, C. Giovanetti-Teixeira, T. Ruchon, T. Auguste, Z. Diveki, P. Breger, A. Maquet, B. Carré, R. Taïeb, and P. Salières, Nature Phys. **6**, 200 (2010).
[22] Z. Diveki, A. Camper, S. Haessler, T. Auguste, T. Ruchon, B. Carré, P. Salières, R. Guichard, J. Caillat, A. Maquet, and R. Taïeb, New J. Phys. **14**, 023062 (2012).
[23] J. Itatani, J. Levesque, D. Zeidler, H. Niikura, H. Pépin, J. C. Kieffer, P. B. Corkum, and D. M. Villeneuve, Nature (London) **432**, 867 (2004).
[24] C. Jin, J. B. Bertrand, R. R. Lucchese, H. J. Wörner, P. B. Corkum, D. M. Villeneuve, A.-T. Le, and C. D. Lin, Phys. Rev. A **85**, 013405 (2012).
[25] H. Park, Z. Wang, H. Xiong, S. B. Schoun, J. Xu, P. Agostini, and L. F. DiMauro, Phys. Rev. Lett. **113**, 263401 (2014).
[26] P. M. Paul, E. S. Toma, P. Breger, G. Mullot, F. Augé, P. Balcou, H. G. Muller, and P. Agostini, Science **292**, 1689 (2001).
[27] H. G. Muller, Appl. Phys. B **74**, S17 (2002).

[28] P. Kruit and F. H. Read, J. Phys. E **16**, 313 (1983).
[29] J. P. Cryan, P. H. Bucksbaum, and R. N. Coffee, Phys. Rev. A **80**, 063412 (2009).
[30] B. K. McFarland, J. P. Farrell, P. H. Bucksbaum, and M. Gühr, Science **322**, 1232 (2008).
[31] G. H. Lee, I. J. Kim, S. B. Park, T. K. Kim, Y. S. Lee, and C. H. Nam, J. Phys. B **43**, 205602 (2010).
[32] See Supplemental Material [url], which includes Refs. [33-43].
[33] M. Wells and R. R. Lucchese, J. Chem. Phys. **110**, 6365 (1999).
[34] S. J. Desjardins, A. D. O. Bawagan, Z. F. Liu, K. H. Tan, Y. Wang, and E. R. Davidson, J. Chem. Phys. **102**, 6385 (1995).
[35] H.-J. Werner, *et al.* MOLPRO, version 2015.1, a package of ab initio programs. (2015) http://www.molpro.net.
[36] H.-J. Werner, P. J. Knowles, G. Knizia, F. R. Manby, and M. Schütz, WIREs Comput. Mol. Sci. **2**, 242 (2012).
[37] K. P. Huber, and G. Herzberg, Molecular spectra and molecular structure IV. constants of diatomic molecules. (Van Nostrand Reinhold Co., New York, 1979).
[38] R. A. Kendall, T. H. Dunning Jr., and R. J. Harrison, J. Chem. Phys. **96**, 6796 (1992).
[39] T. H. Dunning. Jr., J. Chem. Phys. **90**, 1007 (1989).
[40] M. Ehara, M. Ishida, and H. Nakatsuji, Collect. Czech. Chem. Commun. **70**, 881 (2005).
[41] S. Svensson, *et al.*, Phys. Scr. **44**, 184 (1991).
[42] R. E. Stratmann, R. W. Zurales, and R. R. Lucchese, J. Chem. Phys. **104**, 8989 (1996).
[43] R. E. Stratmann, and R. R. Lucchese, J. Chem. Phys. **102**, 8493 (1995).
[44] R. R. Lucchese, G. Raseev, and V. McKoy, Phys. Rev. A **25**, 2572 (1982).
[45] R. E. Stratmann, G. Bandarage, and R. R. Lucchese, Phys. Rev. A **51**, 3756 (1995).
[46] D. Pavičić, K. F. Lee, D. M. Rayner, P. B. Corkum, and D. M. Villeneuve, Phys. Rev. Lett. **98**, 243001 (2007).
[47] D. Pinkham, T. Vogt, and R. R. Jones, J. Chem. Phys. **129**, 064307 (2008).
[48] J. B. Bertrand, H. J. Wörner, P. Hockett, D. M. Villeneuve, and P. B. Corkum, Phys. Rev. Lett. **109**, 143001 (2012).
[49] X. Ren, V. Makhija, A.-T. Le, J. Troß, S. Mondal, C. Jin, V. Kumarappan, and C. Trallero-Herrero, Phys. Rev. A **88**, 043421 (2013).
[50] M. Kotur, D. Guénot, Á. Jiménez-Galán, D. Kroon, E. Larsen, M. Louisy, S. Bengtsson, M. Miranda, J. Mauritsson, C. Arnold, S. Canton, M. Gisselbrecht, T. Carette, J. Dahlström, E. Lindroth, A. Maquet, L. Argenti, F. Martín, and A. L'Huillier, Nat. Commun. **7**, 10566 (2016).
[51] A. Camper, A. Ferré, N. Lin, E. Skantzakis, D. Staedter, E. English, B. Manschwetus, F. Burgy, S. Petit, D. Descamps, T. Auguste, O. Gobert, B. Carré, P. Salières, Y. Mairesse, and T. Ruchon, Photonics **2**, 184 (2015).
[52] A.-T. Le, R. R. Lucchese, and C. D. Lin, Phys. Rev. A **82**, 023814 (2010).
[53] J. L. Dehmer, D. Dill, and S. Wallace, Phys. Rev. Lett. **43**, 1005 (1979).
[54] J. A. Stephens and D. Dill, Phys. Rev. A **31**, 1968 (1985).
[55] B. Basden and R. R. Lucchese, Phys. Rev. A **37**, 89 (1988).
[56] T. A. Ferrett, D. W. Lindle, P. A. Heimann, M. N. Piancastelli, P. H. Kobrin, H. G. Kerkhoff, U. Becker, W. D. Brewer, and D. A. Shirley, J. Chem. Phys. **89**, 4726 (1988).